Infrared Spectral Microimaging
A New Tool to Characterise the Tissue Features in Skin Cancers of Melanoma Type

David Sebiskveradze[1], Cyril Gobinet[1], Nathalie Cardot-Leccia[2], Michel Manfait[1], Pierre Jeannesson[1], Vincent Vuiblet[3] and Olivier Piot[1]

[1]*CNRS FRE 3481 MEDyC, Faculté de Pharmacie, Université de Reims, 51 rue Cognacq-Jay, Reims, France*
[2]*Laboratoire Central d'Anatomo Pathologie, Hopital Pasteur, Centre Hospitalier Universitaire de Nice, Nice, France*
[3]*Laboratoire Pol Bouin, Hopital Maison Blanche, Centre Hospitalier Universitaire de Reims, Reims, France*

Keywords: Melanoma, Skin Cancer, Infrared Spectroscopy, Spectral Imaging, Interconnection of Tissue Structures.

Abstract: Infrared (IR) spectral microimaging is a label-free optical technique that permits to probe the intrinsic chemical composition of biological samples. This technique appears more informative than conventional histology and could be developed as a non-destructive and objective diagnostic tool for in routine use in pathology departments. The discrimination between tumoral and neighbouring tissues relies on highlighting subtle spectral differences by means of advanced statistical multivariate data processing. In this way, we applied an innovative algorithm based on fuzzy clustering to take into account the notion of nuance into the clustering of IR image pixels. IR spectral imaging of human cutaneous melanomas was performed on paraffin-embedded tissue sections, without previous chemical dewaxing. Reconstructed colour-coded images allow recovering automatically different histological structures, by distinguishing tumour from the connective tissue. This approach gives also access to information about the tissue structures. Indeed, it permits to highlight the interconnection between neighbouring structures. In this work in progress study, the analysis was focussed on the interconnection between the tumoral and peritumoral structures and between the tumoral areas in case of a heterogeneous lesion. These first encouraging results pave the way to access new diagnostic and prognostic criteria associated to the tumour aggressiveness in cutaneous melanomas.

1 INTRODUCTION

Melanoma skin cancer is one of the most aggressive human cancers (Chin, 2006; Miller, 2006) and reveals itself as a quiet, but rapid invasive life threatening tumour (Simionescu, 2006). Melanoma incidence rates have been increasing for at least 30 years. Between 2005 and 2009, incidence rates among light skin people increased by 2.8 % per year. In the United States, for example, melanoma is expected to be diagnosed in about 76,690 persons in 2013, accounting for less than 5 % of all skin cancer cases but the vast majority of skin cancer deaths (Cancer Facts & Figures, 2013).

Accurate clinical diagnosis of malignant melanoma is thus of great importance for early detection and further treatment. Generally, the diagnosis is based on the histological evaluation of the lesion (Marghoob, 2009). However, morphological interpretation might be considered as subjective and could result in disagreements in the diagnosis (Urso, 2005; Glusac, 2003). Many attempts in the development of objective automatic image analysis software were realised but due to the complexity of histological structures, results have not yet been conclusive (Gerger, 2003).

Fourier transform mid-infrared (FT–IR) microspectroscopy is an efficient label-free optical method based on the interaction between an infrared (IR) radiation and matter. This vibrational spectroscopy permits to probe the biochemical composition of a sample in a very sensitive, non-destructive, non-invasive and objective manner. Coupled with an imaging system, FT–IR microspectroscopy of human tissues has demonstrated potential to provide clinically relevant diagnostic information in oncology (Krishna, 2007; Wolthuis, 2008; Kong, 2010), and particularly in

Sebiskveradze D., Gobinet C., Cardot-Leccia N., Manfait M., Jeannesson P., Vuiblet V. and Piot O..
Infrared Spectral Microimaging - A New Tool to Characterise the Tissue Features in Skin Cancers of Melanoma Type.
DOI: 10.5220/0004893000590065
In *Proceedings of the International Conference on Bioimaging* (BIOIMAGING-2014), pages 59-65
ISBN: 978-989-758-014-7

detection and characterisation of skin cancers (Ly, 2009). Notably, the possibility to diagnose melanoma from normal epidermis (Mordechai, 2004; Hammody, 2008) or to discriminate between melanoma and benign nevus (Tfayli, 2005) based on the IR markers specific to each tissue type was shown. Associating with multivariate statistical analysis methods, FT-IR imaging has also demonstrated its potential for characterising various melanoma types and highlighting intratumoral heterogeneities within the primary melanoma skin cancers independently of conventional histology (Ly, 2010).

However, the latest developments in IR spectral data processing and pattern recognition methods have permitted highlighting, in skin carcinoma lesions, the subtle biochemical changes between cancerous and surrounding tissue areas (Sebiskveradze, 2011). In this proof of concept study, our objective was to develop an automated digital staining of tissue sections in order to investigate the interconnection between the tumoral and the neighbouring peritumoral areas in primary melanoma. The processing method was based on fuzzy clustering of IR data and on the measure of the cluster intercorrelation.

To this end, two representative samples of good and bad prognosis melanoma were analysed. The IR spectral images were directly collected on paraffin-embedded thin sections and then automatically clustered using an fuzzy clustering algorithm. Moreover, in order to highlight interfaces between the different clusters, a cluster interconnection measure was introduced.

2 MATERIALS AND METHODS

2.1 Patients and Sample Preparation

Two samples of primary cutaneous superficial spreading melanomas (SSM) were analysed in this study. The first one, of good prognosis, developed on the arm of a 65 years old woman, without ulceration, with Clark level of 3 and 0.76 mm Breslow thickness. While, the second one, of bad prognosis, developed on the back of a 55 years old man, presented an invasive nodular component and ulceration, with Clark level of 4 and 2 mm Breslow thickness.

The tissue samples were selected by the pathologists from the tumour bank of the Pathology Department. The specimens were fixed in formalin and paraffin-embedded. From the samples, 10-micron thick slices were cut and mounted on a calcium fluoride (CaF_2) (Crystran Ltd, Dorset, UK) window for FT–IR imaging without any particular preparation, especially no chemical dewaxing. First adjacent slices (5 µm thick) to those used for FT–IR analysis were stained with hematoxylin and eosin (HE) for conventional histology.

2.2 FT-IR Data Acquisition

FT–IR spectral images were recorded in transmission mode with a Spectrum Spotlight 300 FT–IR imaging system coupled to a Spectrum One FT–IR spectrometer (both from PerkinElmer Life Sciences, Waltham, MA, U.S.A.). The spatial resolution of about ten micron and a spectral resolution of 2 cm^{-1} permitted the recording of detailed tissular structures. Before each acquisition, a reference spectrum of the atmospheric environment and the CaF_2 window was recorded. This reference spectrum was subsequently automatically subtracted from the data by a built-in function from the Perkin Elmer Spotlight software. Each spectral image of about 1 mm^2 area, covering a substantial part of the biopsy, consisted of around 30,000 spectra. Each image pixel represents an IR spectrum, which is the absorbance of one measurement point (6.25 × 6.25 μm^2) over 902 wavenumbers uniformly distributed between 900 and 1800 cm^{-1}. This spectral range, characterised as the fingerprint region, actually corresponds to the most informative region for biological samples (Ly, 2008; Ly, 2009).

2.3 Data Pre-processing

Data processing was carried out directly on spectral images using built in-house programs written in Matlab 2008a (The Mathworks, Natick, MA, U.S.A.).

As the samples were analysed without previous chemical dewaxing, the recorded FT–IR spectral images had to be digitally corrected for paraffin spectral contribution. To achieve this goal, an automated pre-processing method based on extended multiplicative signal correction (EMSC) was applied on each recorded data set. This method has already shown its digital dewaxing potential on skin and colon cancer samples (Ly, 2008; Wolthuis, 2008). Briefly, the mean spectrum was computed by averaging all recorded spectra of each image. Light scattering effects were modelled with a fourth-order polynomial function. In order to take into account the spectral variability of paraffin, the interference

matrix of the model was composed of the average spectrum of paraffin and the first nine principal components extracted from a FT–IR spectral image recorded on a pure paraffin block. After the application of the EMSC-based pre-processing, paraffin contribution was neutralized, thus permitting to retain in the data sets only the spectral variability of the tissue.

In addition, this pre-processing step permitted to discard from the analysis outliers and poor tissue signal to noise ratio spectra. On the pseudo-colour clustering images, the corresponding pixels are white coloured for better visualisation.

2.4 Fuzzy Clustering

The spectral differences between different skin structures (such as dermis, epidermis and tumour) are weak after the EMSC-based pre-processing step. To highlight the different biological structures of the analysed sample, clustering methods can be used. The main objective of clustering is to group together similar spectra in order to reveal areas of interest within tissue sections. In IR spectral imaging of cancerous tissues, clustering methods allow to create highly contrasted pseudo-colour images permitting to localize tumoral nests within a complex tissue (Ly, 2009; Sebiskveradze, 2011).

For each spectral image, a clustering method based on fuzzy C-means (FCM) was used. One of the particularities of FCM clustering is that it permits to assign each pixel (spectrum) to every cluster with an associated membership value varying between 0 and 1; the sum of all the cluster membership values for one pixel being equal to 1 (Bezdek, 1981). The amount of fuzziness introduced in the clustering is managed by the fuzzy parameter. Increasing the value of this parameter induces more fuzziness in the clustering. Classical FCM algorithm is considered as unsupervised except for the number of clusters and the fuzziness parameter, determined by the operator. Here, we used an algorithm named RBA (Redundancy-Based Algorithm) to automatically determine both FCM parameters (Sebiskveradze, 2011).

In this study, we applied the FCM function from the Matlab Statistics Toolbox with the Euclidean distance. For each cluster, the cluster-membership information was plotted in a separate image as a pseudo-colour map. For cluster assignment, each pseudo-colour map was then provided to the pathologists for a comparison with the corresponding HE-stained sections.

2.5 Measure of Interconnection between Spectral Clusters

Interconnection corresponds to the sample areas (or image pixels) shared between two clusters. To calculate this interconnection the following mathematical equation was implemented:

$$M_{ij}(n) = -\left(\frac{u_{in}}{u_{in}+u_{jn}} \frac{\log\left(\frac{u_{in}}{u_{in}+u_{jn}}\right)}{\log 2} + \frac{u_{jn}}{u_{in}+u_{jn}} \frac{\log\left(\frac{u_{jn}}{u_{in}+u_{jn}}\right)}{\log 2} \right) \frac{u_{in}u_{jn}}{\left(\frac{1}{2}\right)^2}$$

where $M_{ij}(n)$ represents the interconnection measurement calculated between i and j clusters for the given pixel n; while, u_{in} and u_{jn} are respectively i and j cluster membership values for this pixel. This interconnection value varies between 0 (no overlapping between the two clusters) and 1 (uniform distribution of pixel membership value between the two clusters).

3 RESULTS AND DISCUSSION

The IR spectral images recorded on each tissue section contained approximately 30,000 spectra. These spectra were pre-processed in order to remove paraffin contribution and clustered using the FCM-based algorithm to regroup, within the same image, spectra that show similar bio-molecular properties. Note that for each case the number of clusters was determined automatically by the algorithm. On the analysed samples, it was possible to establish a one-to-one correlation from those highly contrasted FCM images to the adjacent HE section.

Figure 1 corresponds to the FCM-based algorithm images obtained from the non-ulcerated SSM (patient 1). Instead of superimposing the images, each cluster was presented into a separate pseudo-colour image. Here, we considered that the pixels belonging significantly to a cluster image presented a membership value superior to 0.4. Thus, the clusters were assigned as follow: keratin (cluster 1), epidermis (cluster 2), tumour (cluster 3), peritumoral collagen (clusters 4 and 5), lymphocytes (cluster 6) and deep dermis (clusters 7 and 8).

Figure 2 depicts the images obtained from an ulcerated SSM with an invasive nodular component (patient 2). In this example, six clusters obtained by FCM-based algorithm were assigned to the following tissular structures: two distinctive types of

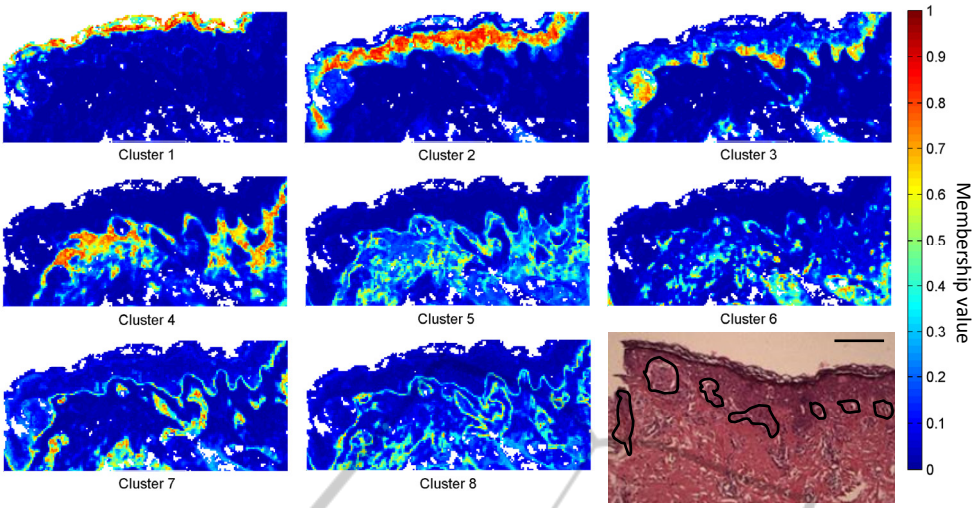

Figure 1: Spectral histology obtained from a non-ulcerated superficial spreading melanoma (patient 1) using FCM-based algorithm. Pseudo-colour map built with 8 clusters represented by individual images with corresponding hematoxylin and eosin-stained image (scale bar, 200 µm, tumour is outlined). Assignment of the clusters: keratin (1), epidermis (2), tumour (3), peritumoral collagen (4 and 5), lymphocytes (6) and deep dermis (7 and 8).

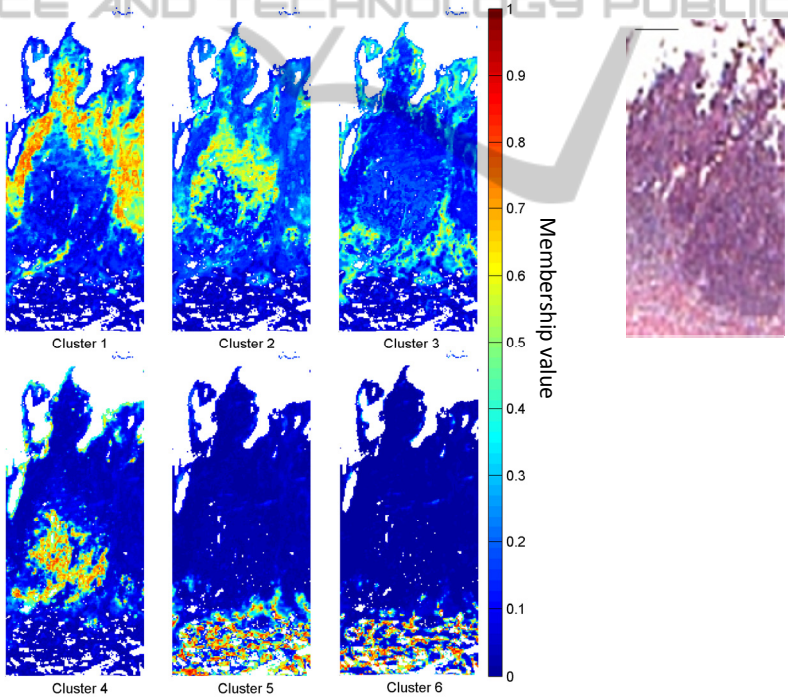

Figure 2: Spectral histology obtained from an ulcerated superficial spreading melanoma with an invasive nodular component (patient 2) using FCM-based algorithm. Pseudo-colour map built with 6 clusters represented by individual images with corresponding hematoxylin and eosin-stained image (scale bar, 200 µm). Assignment of the clusters: tumour (1 and 2), intratumoral collagen (3), lymphocytes (4), deep collagen (5 and 6).

tumour cells (clusters 1 and 2) were located in the invasive component. The intratumoral collagen (cluster 3) also appeared. Other structures represented by the clusters 5 and 6 were assigned to deep collagen. Furthermore, very detailed histological structures such as lymphocytes can be recovered (cluster 4) indicating the presence of an inflammatory component.

As visible from the presented samples, in both cases, tumours were very well delineated and demarcated from the epidermis. Moreover, the first one corresponding to a good prognosis melanoma contained only one tumour cluster while for the second one of bad prognosis (i.e. presenting a metastatic risk), a tumoral heterogeneity was revealed by the identification of 2 clusters (Okcu, 1996).

After this first processing of spectral data permitting to recover the histological organisation of the tissue, we applied the new spectral interconnection measure between the identified clusters. Indeed, for each pixel, an interconnection value was calculated for a couple of clusters of interest. As a result, the generated new images, presenting the same spatial size, were displayed according to a colorbar scale from 0 (no interconnection between the clusters, dark-colour pixels) and 1 (maximum of interconnection, light-coloured pixels). For the analysed samples, different circumstances can be observed.

Figure 3 shows the interconnection between the tumour cluster and its surrounding structures for the non-ulcerated SSM (patient 1) whose FCM clusters are indicated in Figure 1. Indeed, through the Figure 3A we can assume the high interconnection between the tumour cluster (cluster 3) and the neighbouring epidermis (cluster 2). In addition, Figures 3B and 3C show a low interconnection between the tumour and the peritumoral collagen (clusters 4 and 5). Similar calculations were performed for the ulcerated SSM which presents an invasive nodular component (patient 2) (Figure 4). Indeed, Figure 4A revealed a maximal interconnection between the two different types of tumour clusters (clusters 1 and 2 of Figure 2). Further, on the Figures 4B and 4C, a high interconnection was highlighted between these tumour clusters and their microenvironment corresponding to intratumoral collagen (cluster 3). Highlighting such interconnection between the invasive tumour and its surrounding tissue confirms the hypothesis that strong interactions exist between the tumour cells and their matrix environment.

Moreover, a marked interconnection between one type of tumour cells (cluster 2), located in the invasive region of the malignant lesion, and the inflammatory component (cluster 4) was identified (Figure 4D). This cluster assigned to the inflammation does not present any interconnection with the other tumour cluster (cluster 1) (data not shown). An absence of interconnection was also noticed between the tumour and the deep collagen, (clusters 5 and 6 of Figure 2) (data not shown).

The obtained results demonstrate the feasibility of FT-IR spectral imaging associated with advanced multivariate statistical analyses as a powerful automatic tool for histopathological characterisation of primary cutaneous melanoma. The efficiency of this biophotonic imaging technique relies on its capability to probe the subtle differences of molecular composition that exist between the tissue structures.

Moreover, the highlighting of novel spectral marker of tumour invasiveness reinforces the idea of integration of this approach in the conventional morphological analyses in order to help in the guidance of therapeutic diagnoses.

4 CONCLUSIONS

The combination of IR imaging and pattern recognition techniques might be an innovative, label-free, high-throughput and automatic technology to aid screening high-risk metastatic melanoma lesions at their earliest stages. Moreover, from the histopathological point of view, highlighting an invasive component in melanoma skin cancer is of great interest, since it permits to determine the precise area where the invasive cells can infiltrate the surrounding tissue. This kind of invasive front is of crucial importance to assess the

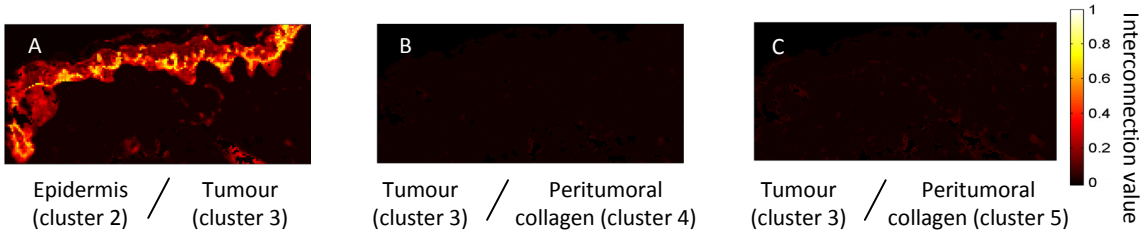

Figure 3: Illustration of interconnection measurements for a non-ulcerated superficial spreading melanoma (patient 1). 3 circumstances: A) between the tumour and epidermis clusters, B) and C) between the tumour and peritumoral collagen clusters.

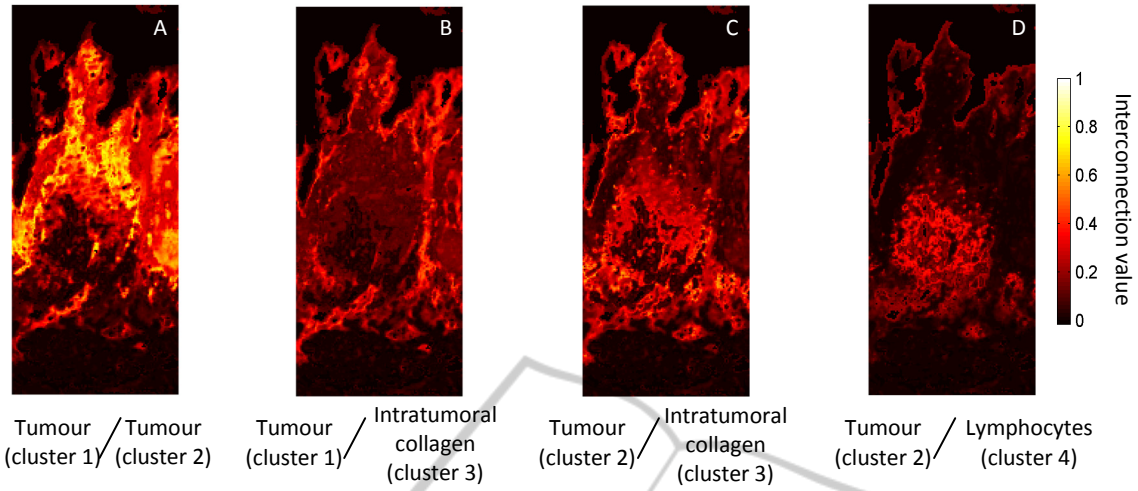

Figure 4: Illustration of interconnection measurements for an ulcerated superficial spreading melanoma with an invasive nodular component (patient 2). 4 circumstances: A) between the tumour clusters, B) and C) between tumours and intratumoral collagen clusters, D) between tumour and lymphocytes clusters.

tumour agressiveness, by revealing a risk of malignant cell escape and consequently metastasis formation. These first results need to be validated by further analysis on a large number of samples, before envisaging a potential application in clinics.

REFERENCES

Bezdek, J. C., 1981. *Pattern recognition with fuzzy objective function algorithms,* Plenum Press. New York.

Cancer Facts and Figures, 2013. *American Cancer Society,* Atlanta.

Chin, L., Garraway, L. A., and Fisher, D. E., 2006. Malignant melanoma: genetics and therapeutics in the genomic era. *Genes and development*, vol. 20, pp. 2149-2182.

Gerger, A., Smolle, J., 2003. Diagnostic imaging of melanocytic skin tumors. *Journal of cutaneous pathology,* vol. 30, pp. 247-252.

Glusac, E. J., 2003. Under the microscope: doctors, lawyers, and melanocytic neoplasms. *Journal of cutaneous pathology,* vol. 30, pp. 287-293.

Hammody, Z., Argov, S., Sahu, R. K., Cagnano, E., Moreh, R., and Mordechai, S., 2008. Distinction of malignant melanoma and epidermis using IR micro-spectroscopy and statistical methods. *Analyst,* vol. 133, pp. 372-378.

Kong, R., Reddy, R. K., and Bhargava, R., 2010. Characterization of tumor progression in engineered tissue using infrared spectroscopic imaging. *Analyst,* vol. 135, pp. 1569-1578.

Krishna, C. M., Sockalingum, G. D., Bhat, R. A., Venteo, L., Kushtagi, P., Pluot, M., and Manfait, M., 2007. FTIR and Raman microspectroscopy of normal, benign, and malignant formalin-fixed ovarian tissues. *Analytical and Bioanalytical Chemistry,* vol. 387, pp. 1649–1656.

Ly, E., Piot, O., Wolthuis, R., Durlach, A., Bernard, P., and Manfait, M., 2008. Combination of FTIR spectral imaging and chemometrics for tumour detection from paraffin-embedded biopsies. *Analyst,* vol. 133, pp. 197-205.

Ly, E., Piot, O., Durlach, A., Bernard, P., and Manfait, M., 2009. Differential diagnosis of cutaneous carcinomas by infrared spectral micro-imaging combined with pattern recognition. *Analyst,* vol. 134, pp. 1208-1214.

Ly, E., Cardot-Leccia, N., Ortonne, J. P., Benchetrit, M., Michiels, J. F., Manfait, M., and Piot, O., 2010. Histopathological characterization of primary cutaneous melanoma using infrared microimaging: a proof-of-concept study. *British Journal of Dermatology,* vol. 162, pp. 1316-1323.

Marghoob, A. A., Scope, A., 2009. The complexity of diagnosing melanoma. *Journal of Investigative Dermatology,* vol. 129, pp. 11-13.

Miller, A. J., Mihm Jr, M. C., 2006. Melanoma. *New England Journal of Medicine,* vol. 355, pp. 51-65.

Mordechai, S., Sahu, R. K., Hammody, Z., Mark, S., Kantarovich, K., Guterman, H., PODSHYVALOV, A., GOLDSTEIN, J., and Argov, S., 2004. Possible common biomarkers from FTIR microspectroscopy of cervical cancer and melanoma. *Journal of microscopy,* vol. 215, pp. 86-91.

Okcu, A., Hofmann-Wellenhof, R., Woltsche, I., Smolle, J., and Kerl, H., 1996. Pathological findings suggestive of interclonal stabilization in a case of cutaneous melanoma. *Clinical and experimental metastasis,* vol. 14, pp. 215-218.

Sebiskveradze, D., Vrabie, V., Gobinet, C., Durlach, A., Bernard, P., Ly, E., Manfait, M., Jeannesson, P., and Piot, O., 2011. Automation of an algorithm based on fuzzy clustering for analyzing tumoral heterogeneity in

human skin carcinoma tissue sections. *Laboratory Investigation,* vol. 91, pp. 799-811.

Simionescu, O., Costache, M., and Testori, A., 2006. Cutaneous melanoma: digital dermoscopy-essential tool for positive diagnosis. *Journal of cellular and molecular medicine,* vol. 10, pp. 991-994.

Tfayli, A., Piot, O., Durlach, A., Bernard, P., and Manfait, M., 2005. Discriminating nevus and melanoma on paraffin-embedded skin biopsies using FTIR microspectroscopy. *Biochimica et Biophysica Acta (BBA)-General Subjects,* vol. 1724, pp. 262-269.

Urso, C., Rongioletti, F., Innocenzi, D., Saieva, C., Batolo, D., Chimenti, S., Filotico, R., Gianotti, R., Lentini, M., Tomasini, C., Rebora, A., and Pippione, M., 2005. Interobserver reproducibility of histological features in cutaneous malignant melanoma. *Journal of clinical pathology,* vol. 58, pp. 1194-1198.

Wolthuis, R., Travo, A., Nicolet, C., Neuville, A., Gaub, M. P., Guenot, D., Ly, E., Manfait, M., Jeannesson, P., and Piot, O., 2008. IR spectral imaging for histopathological characterization of xenografted human colon carcinomas. *Analytical chemistry,* vol. 80, pp. 8461-8469.